Correlated Sample-Based Prior in Bayesian Inversion Framework for Microwave Tomography

Rahul Yadav, Adel Omrani, Guido Link, Marko Vauhkonen, and Timo Lähivaara

***Abstract*— When using the statistical inversion framework in microwave tomography (MWT), generally, the real and imaginary parts of the unknown dielectric constant are treated as uncorrelated and independent random variables. Thereby, in the maximum *a posteriori* estimates, the two recovered variables may show different structural changes inside the imaging domain. In this work, a correlated sample-based prior model is presented to incorporate the correlation of the real part with the imaginary part of the dielectric constant in the statistical inversion framework. The method is used to estimate the inhomogeneous moisture distribution (as dielectric constant) in a large cross section of polymer foam. The targeted application of MWT is in industrial drying to derive intelligent control methods based on tomographic inputs for selective heating purposes. One of the features of the proposed method shows how to integrate lab-based dielectric characterization, often available in MWT application cases, in the prior modeling. The method is validated with numerical and experimental MWT data for the considered moisture distributions.**

***Index Terms*— Correlated sample-based prior, industrial microwave drying, maximum *a posteriori*, microwave tomography, statistical inversion method.**

I. Introduction

MICROWAVE tomography (MWT) use-cases in the industry are mostly for monitoring and inspection purposes, as reported in [1]–[3]. A new idea is to apply MWT based control in the industrial microwave heating system [4], known as HEPHAISTOS [5], to increase its heating efficiency and enhance the material processing quality. The HEPHAISTOS system has a hexagonal design [6] for the applicator (cavity) that offers a very high uniform electromagnetic field inside the cavity. Its main areas of applications are in material processing, for example, drying, sintering, and thermal curing. Often, this system suffers from the problem of hot-spot formation and overheating (thermal runaway) specifically while drying materials with low-loss like porous polymer foam. These situations may degrade the quality of material processing or may even lead to damage to the industrial unit.

One of the solutions to eliminate the problem of thermal runaway and hot-spot formation is intelligent control of power sources (magnetrons) to obtain a selective heating rate at each stage of the drying process [7], [8]. However, to apply such a precise microwave power control *in situ* and noninvasive measurement of the unknown distribution of moisture inside the porous material is required. The infrared camera sensors integrated with the microwave drying systems for process observation are limited to providing information on the material's surface only and, hence, not adequate to provide efficient control of microwave power sources. Thus, integration of MWT imaging modality [9], [10] with the drying system was proposed to estimate the moisture content distribution in a polymer foam. Using the MWT tomographic output, strategies for intelligent control can be derived. The MWT senor setup consists of open-ended waveguide antennas operating in the X-band range. The selection of the frequency and the antenna type for the MWT sensor array are detailed in [11]. For estimating the moisture levels (in terms of dielectric constant) in a porous material with a large cross-sectional dimension, we apply a statistical inversion approach [12] based on the Bayesian framework. Some earlier efforts of using statistical inversion approaches in MWT have been proposed in [13]–[16].

In our earlier studies [17], [18] on statistical inversion in MWT, the real and imaginary parts of the unknown dielectric constant were treated as independent and uncorrelated random variables. This assumption led to independent reconstructions of the real and imaginary parts, causing conflicting and incorrect moisture level estimates by the real and imaginary parts. As the imaginary part governs the heating behavior, its correct estimation becomes imperative when deriving optimal control algorithms for the drying system. Therefore, to achieve accurate maximum *a posteriori* estimates (MAP), the key is to construct a joint-prior model that favors correlation between the real and imaginary parts. In [19] and [20], a similar problem is addressed using the expectation–maximization (EM) algorithm [21], albeit it may not be a suitable approach for our high-dimensional problem with a nonlinear observation model.

Manuscript received 27 April 2021; revised 13 October 2021; accepted 3 January 2022. Date of publication 28 January 2022; date of current version 26 July 2022. This work was supported in part by the Academy of Finland (Finnish Centre of Excellence of Inverse Modeling and Imaging) under Project 312344 and Project 321761 and in part by the European Union's Horizon 2020 Research and Innovation Program through the Marie Skłodowska-Curie (TOMOCON-www.tomocon.eu) under Grant 764902. *(Corresponding author: Rahul Yadav.)*

Rahul Yadav, Marko Vauhkonen, and Timo Lähivaara are with the Department of Applied Physics, University of Eastern Finland, 70210 Kuopio, Finland (e-mail: rahuly@uef.fi; marko.vauhkonen@uef.fi; timo.lahivaara@uef.fi).

Adel Omrani and Guido Link are with the Institute for Pulsed Power and Microwave Technology, Karlsruhe Institute of Technology, 76344 Karlsruhe, Germany (e-mail: adel.hamzekalaei@kit.edu; guido.link@kit.edu).

Color versions of one or more figures in this article are available at https://doi.org/10.1109/TAP.2022.3145433.

Digital Object Identifier 10.1109/TAP.2022.3145433

On the other hand, joint reconstructions in the deterministic inversion methods have been addressed in: 1) [22] where the complex permittivity in the imaging domain is expressed as a weighted sum of a few pre-selected permittivities, close to the range of the expected values, and permittivity weights are obtained using Gauss–Newton inversion (GNI) algorithm; however, the method is mostly valid for practical biomedical applications with linearized inverse scattering model and 2) in [23] and [24], an approximate ratio is obtained between the real and imaginary parts of the complex permittivity based on the dielectric characterization of the material(s) under test, and this approximate ratio served as the prior information in the GNI algorithm with the total variation multiplicative regularizer term. Moreover, the results show improvement by adjusting the approximate average ratio. However, in our work, the moisture-to-dielectric relationship is nonlinear; thus, a single average factor for all moisture points will lead to inaccurate reconstructions.

In this work, we present a correlated sample-based prior model, as an extension to our preliminary work [25], to construct the prior covariance structure for the joint-prior Gaussian density. The method is primarily suitable for the use-case of MWT when either structural information of the imaging domain or dielectric behavior of the material under test is available *a priori*. For example, in medical applications, the structure of the body organs and their dielectric properties are known approximately. In our MWT application, dielectric characterization of the foam with respect to different moisture levels (wet-basis) is available. To form the prior covariance structure, first, a database containing possible moisture distribution is formed with different spatial variations. The inhomogeneous profile of each sample is modeled using the squared exponential covariance function, and its dielectric values are based on the available dielectric characterization data. Next, the second-order statistics of this database are calculated to build the joint prior covariance structure. Herein, the performance of the proposed correlated sample-based prior model is first evaluated with numerical scattered field data from the 2-D MWT setup for three moisture scenarios. Furthermore, we have also evaluated the sample-based prior model on the scattered electric field data from our developed prototype of the MWT system. Results presented show the efficacy of this approach in comparison to the past approach where parameters are considered uncorrelated.

This article is organized as follows. Section II provides an overview of the MWT setup and the forward observation model. Section III details the statistical inversion framework. Prior construction and sample-based prior model approach are given in Section IV. In Section V, the results for different realistic moisture scenarios are presented using 2-D synthetic data. Experimental results are investigated in Section VI. Finally, Section VII shows the concluding remarks.

II. Microwave Tomography: Setup and Observation Model

In this study, we consider a 2-D imaging domain $\Omega_{\text{foam}} = [-25,\ 25] \times [-1.5,\ 1.5]$ cm with inhomogenous relative dielectric constant $\epsilon_r = \epsilon_r' - j\epsilon_r''$, placed in the background

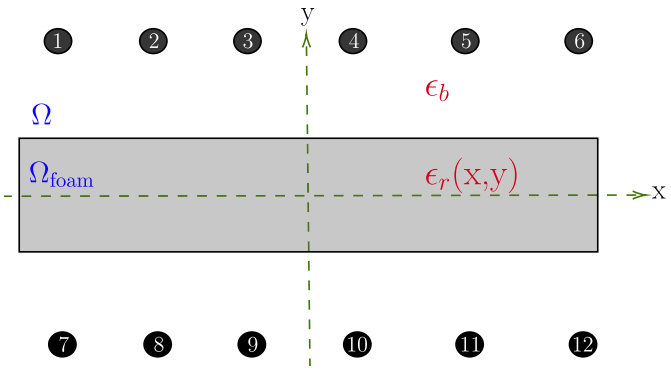

Fig. 1. Schematic of the 2-D MWT setup used in the study.

domain Ω consisting of free-space with $\epsilon_b = 1 - j0$. For this 2-D numerical study, the open-ended waveguide antennas are modeled as a line source with an excitation frequency of 8.3 GHz and are located at a distance of 15 cm from the top and bottom surfaces of the foam. The 2-D MWT setup is shown in Fig. 1 where the sources are represented by number Tags $N = 1, 2, \ldots, 12$. The scattered electric field E^{scat} under the illumination of time-harmonic (time convention $e^{-j\omega t}$ with angular frequency of ω is assumed and suppressed) TM-polarized incident field is given as [26], [27]

$$E^{\text{scat}}(r) = k^2 \int_{\Omega_{\text{foam}}} G(r, r')\left(\epsilon_r(r') - \epsilon_b\right) E_{\text{tot}}(r')\, dr' \qquad \forall r \in \Omega,\quad r' \in \Omega_{\text{foam}} \tag{1}$$

where k is the wavenumber of the background medium and $G(r, r')$ is the background Green's function of 2-D line source (i.e. the Hankel function of the second kind and zeroth order). The observation and source points are denoted by the position vectors $r \mapsto (x, y)$ and $r' \mapsto (x', y')$, respectively. The term E_{tot} is the total electric field inside the domain Ω_{foam} and is calculated as

$$E_{\text{tot}}(r) = E_{\text{inc}}(r) + k^2 \int_{\Omega_{\text{foam}}} G(r, r')\left(\epsilon_r(r') - \epsilon_b\right) E_{\text{tot}}(r')\, dr' \qquad \forall r,\ r' \in \Omega_{\text{foam}} \tag{2}$$

where E_{inc} is the incident electric field.

After discretization [28], [29] for all N transmitter and receiver, (1) is given as

$$E^{\text{scat}} = \mathcal{L}_{\text{o}}(\epsilon_r) E_{\text{tot}} \tag{3}$$

and (2) as

$$E_{\text{tot}} = [\text{I} - \mathcal{L}_{\text{in}}(\epsilon_r)]^{-1} E_{\text{inc}}. \tag{4}$$

Furthermore, by substituting (4) in (3), the scattered electric field can then be expressed as

$$E^{\text{scat}} = \mathcal{L}_{\text{o}}(\epsilon_r)[\text{I} - \mathcal{L}_{\text{in}}(\epsilon_r)]^{-1} E_{\text{inc}} = \mathscr{F}(\epsilon_r) \tag{5}$$

where $\mathcal{L}_0$ and $\mathcal{L}_{\text{in}}$ are short notations for the integral operators in (1) and (2), respectively. This is known as a forward observation model that maps the dielectric constant to scattered electric field where the mapping is denoted by $\mathscr{F}$. As the total electric field depends on the dielectric constant of the foam, its mapping with the scattered electric field is nonlinear.

In (5), the scattered field data can come from real experiment or may be simulated data, while the right-hand side denotes the approximate physical nature of the problem. To obtain estimates using measurement data related to S-parameters, proper calibration scheme can be used to convert the data into electric field [30], [31].

In MWT, the aim is to estimate the 2-D dielectric profile of the porous material given the measurement data E^{scat}. Generally, this is a severely ill-posed inverse problem mainly due to the fact that different profiles may map to the same measurement data. Also, part of the ill-posedness is due to the properties of the integral operator defined in (5) [32]. Under the quantitative inversion framework, the regularization term (related to the prior information) can reduce this problem to some level and improve the estimates. In our case, some prior information related to the dielectric behavior of the foam with respect to wet-basis moisture content level is available. Furthermore, we expect the moisture content distribution to have smooth distribution in the foam. In this work, to naturally encode this information in the regularization term, we apply a statistical inversion approach based on the Bayesian framework. With the Bayesian estimate, it can be quantified which parameters are more favorable to generate the measurement data rather than providing fixed estimates that are given in classical, deterministic, inversion framework.

III. Bayesian Inversion Framework

Consider an inverse problem of identifying an unknown parameter $\epsilon_r \in \mathbb{C}^{m\times n}$ given noisy measurement data $E^{\text{scat}} \in \mathbb{C}^{N\times N}$ according to the observation model [17], [18]

$$E^{\text{scat}} = \mathscr{F}(\epsilon_r) + \xi \tag{6}$$

where ξ denotes the additive measurement noise component. Herein, the unknown parameter and noise terms are considered mutually independent. Note that the unknown parameter and the measurement data are complex quantities and denoted by $\mathbb{C}$. In this article, the real and imaginary parts are treated separately as real-valued random variables for the real-valued optimization problem. They are separated into real and imaginary parts and concatenated in the 2-D vector form as

$$E^{\text{scat}} = \begin{pmatrix} \mathbb{R}\{E^{\text{scat}}\} \\ \mathbb{I}\{E^{\text{scat}}\} \end{pmatrix}_{2S\times 1} \tag{7}$$

and

$$\epsilon_r = \begin{pmatrix} \{\epsilon_{r_i'}\} \\ \{\epsilon_{r_i''}\} \end{pmatrix}_{2N_n\times 1}, \quad i = 1, 2, \ldots, N_n \tag{8}$$

where $S = N \times N$ and $N_n = m \times n$ are the total number of measurements and the total number of unknowns, respectively.

In statistical inversion, we treat the unknown parameters as random variables, and information about them is expressed in terms of probability densities. The inverse problem can then be expressed as given the measurement data, and the task is to find the conditional probability density $\pi(\epsilon_r \mid E^{\text{scat}})$ for the unknown parameter ϵ_r. The conditional probability density is constructed using Bayes' theorem as

$$\begin{aligned} \pi\left(\epsilon_r \mid E^{\text{scat}}\right) &= \frac{\pi\left(E^{\text{scat}} \mid \epsilon_r\right)\pi(\epsilon_r)}{\pi(E^{\text{scat}})} \\ &\propto \pi\left(E^{\text{scat}} \mid \epsilon_r\right)\pi(\epsilon_r) \end{aligned} \tag{9}$$

where $\pi(\epsilon_r \mid E^{\text{scat}})$ is the posterior density, $\pi(E^{\text{scat}} \mid \epsilon_r)$ is the likelihood density that represents the distribution of the measured data if ϵ_r is known, and $\pi(\epsilon_r)$ is the prior density that contains the prior information available for unknown ϵ_r. The denominator is the marginal density of the measured data and plays the role of normalization constant. It is often ignored since it requires integration over all possible ϵ_r space. In the next step, we construct the likelihood and prior density terms and obtain the posterior density.

Let the joint prior model of the unknowns and noise be $\pi(E^{\text{scat}}, \epsilon_r, \xi)$. Using Bayes' theorem repeatedly, the joint distribution of all associated random variables can be decomposed as

$$\begin{aligned} \pi\left(E^{\text{scat}}, \epsilon_r, \xi\right) &= \pi\left(E^{\text{scat}} \mid \epsilon_r, \xi\right)\pi(\xi \mid \epsilon_r)\pi(\epsilon_r) \\ &= \pi\left(E^{\text{scat}}, \xi \mid \epsilon_r\right)\pi(\epsilon_r). \end{aligned} \tag{10}$$

In the case that both ϵ_r and ξ are fixed, the measurement in the model (6) is completely specified, so the conditional density $\pi(E^{\text{scat}} \mid \epsilon_r, \xi)$ is formally given by

$$\pi\left(E^{\text{scat}} \mid \epsilon_r, \xi\right) = \delta\big(E^{\text{scat}} - \mathscr{F}(\epsilon_r) - \xi\big) \tag{11}$$

where δ is the Dirac delta distribution. Using (9)–(11), we get the likelihood model as

$$\begin{aligned} \pi\left(E^{\text{scat}} \mid \epsilon_r\right) &= \int \pi\left(E^{\text{scat}}, \xi \mid \epsilon_r\right) d\xi \\ &= \int \pi\left(E^{\text{scat}} \mid \epsilon_r, \xi\right)\pi(\xi \mid \epsilon_r) d\xi \\ &= \int \delta\big(E^{\text{scat}} - \mathscr{F}(\epsilon_r) - \xi\big)\pi(\xi \mid \epsilon_r) d\xi \\ &= \pi_{\xi|\epsilon_r}\big(\big(E^{\text{scat}} - \mathscr{F}(\epsilon_r)\big) \mid \epsilon_r\big). \end{aligned} \tag{12}$$

In the quite common case of mutually independent ϵ_r and ξ, we have $\pi_{\xi|\epsilon_r}(\xi \mid \epsilon_r) = \pi_\xi(\xi)$, where $\pi_\xi(\cdot)$ denotes the distribution of noise. Furthermore, if the noise is assumed to be additive Gaussian with zero mean and covariance matrix Γ_ξ, the likelihood density can be written as

$$\begin{aligned} \pi\left(E^{\text{scat}} \mid \epsilon_r\right) \propto \exp\Bigg\{ -\frac{1}{2}\big(E^{\text{scat}} - \mathscr{F}(\epsilon_r)\big)^\top \Gamma_\xi^{-1} \\ \times \big(E^{\text{scat}} - \mathscr{F}(\epsilon_r)\big)\Bigg\} \end{aligned} \tag{13}$$

where $(\cdot)^\top$ denotes the transpose operator. Furthermore

$$\begin{aligned} \pi\left(E^{\text{scat}} \mid \epsilon_r\right) \propto \exp\Bigg\{ -\frac{1}{2}\big(E^{\text{scat}} - \mathscr{F}(\epsilon_r)\big)^\top L_\xi^\top L_\xi \\ \times \big(E^{\text{scat}} - \mathscr{F}(\epsilon_r)\big)\Bigg\} \end{aligned} \tag{14}$$

which can then be written in the norm form as

$$\pi\left(E^{\text{scat}} \mid \epsilon_r\right) \propto \exp\left\{ -\frac{1}{2}\left\| L_\xi\big(E^{\text{scat}} - \mathscr{F}(\epsilon_r)\big)\right\|^2 \right\} \tag{15}$$

where L_ξ is the Cholesky factor of the inverse of the noise covariance matrix. As a prior information, it is first assumed that the moisture variation is smooth inside the foam. Such an assumption can be encoded using a Gaussian density with mean η_{ϵ_r} and covariance Γ_{ϵ_r} as

$$\pi(\epsilon_r) \propto \exp\left\{-\frac{1}{2}\left(\epsilon_r - \eta_{\epsilon_r}\right)^\top \Gamma_{\epsilon_r}^{-1}\left(\epsilon_r - \eta_{\epsilon_r}\right)\right\} = \exp\left\{-\frac{1}{2}\left\|L_{\epsilon_r}\left(\epsilon_r - \eta_{\epsilon_r}\right)\right\|^2\right\}. \quad (16)$$

Here, L_{ϵ_r} is the Cholesky factor of the inverse of the prior covariance matrix Γ_{ϵ_r}. The prior covariance matrix encodes the spatial smoothness knowledge of the unknowns. After multiplying the expressions in (15) and (16) and ignoring the normalization constant in (9), posterior density is obtained that contains the complete solution of the inverse problem in the Bayesian framework and can be expressed by point estimates. One of the most common point estimates in tomographic imaging problems is the *maximum a posteriori* (MAP). The MAP estimate can be computed from the posterior as

$$\widehat{\epsilon}_{r_{\text{MAP}}} = \arg\max_{\epsilon_r} \pi\left(\epsilon_r \mid E^{\text{scat}}\right). \quad (17)$$

This problem is equivalent to the minimization problem

$$\widehat{\epsilon}_{r_{\text{MAP}}} = \arg\min_{\epsilon_r}\left\{\left\|L_\xi\left(E^{\text{scat}} - \mathscr{F}(\epsilon_r)\right)\right\|^2 + \left\|L_{\epsilon_r}\left(\epsilon_r - \eta_{\epsilon_r}\right)\right\|^2\right\} \quad (18)$$

which is a regularized nonlinear least-square (LS) problem. In (18), the prior norm term acts as a regularization term, and it shares close links to generalized Tikhonov regularization. This minimization problem can be formally solved using the gradient-based optimization method. In the Newton-type method, the minimum point is found iteratively by linearizing the forward model, resulting in a linear LS solution in each iteration as

$$\epsilon_{r_{\ell+1}} = \epsilon_{r_\ell} + \alpha_\ell A^{-1} B \quad (19)$$

with

$$A = \left(J_\ell^T \Gamma_\xi^{-1} J_\ell + \Gamma_{\epsilon_r}^{-1}\right)$$
$$B = \left(J_\ell^T \Gamma_\xi^{-1}\left(E^{\text{scat}} - \mathscr{F}\left(\epsilon_{r_\ell}\right)\right) - \Gamma_{\epsilon_r}^{-1}\left(\epsilon_{r_\ell} - \eta_{\epsilon_r}\right)\right)$$

where α_ℓ is the step length parameter, index ℓ is the iteration number, and J_ℓ is a Jacobian matrix (its derivation can be found in [33]), which is decomposed in real ($J_\mathbb{R}$) and imaginary ($J_\mathbb{I}$) parts as

$$J = \begin{bmatrix} J_\mathbb{R} & J_\mathbb{I} \\ -J_\mathbb{I} & J_\mathbb{R} \end{bmatrix}_{2S \times 2N_n}.$$

The approximate covariance of the posterior density Γ_{post} is given as

$$\Gamma_{\text{post}} = \left(J_\ell^T \Gamma_\xi^{-1} J_\ell + \Gamma_{\epsilon_r}^{-1}\right)^{-1}. \quad (20)$$

This approximate posterior indicates the uncertainty associated with the ill-posedness of the solution.

A. Noise Model

Let us denote the noise standard deviations (STD) of the real and imaginary parts of the complex-valued scattered electric field data to be $\sigma_\mathbb{R}$ and $\sigma_\mathbb{I}$, respectively. Under the assumption that noise between measurement points is independent and not correlated, the noise covariance is then given as

$$\Gamma_\xi = \begin{bmatrix} \sigma_\mathbb{R}^2 \mathrm{I}_S & 0_S \\ 0_S & \sigma_\mathbb{I}^2 \mathrm{I}_S \end{bmatrix} \quad (21)$$

where I_S is an $S \times S$ identity matrix and 0_S is an $S \times S$ zero matrix. In the case of real measurements, the noise covariance can be estimated by performing repeated measurements.

IV. Prior Modeling

In Section III, we defined the general expression for the prior density in (16). Since the unknown complex-valued dielectric constant is treated as a real-valued random variable, the prior density in (16) can be further expressed [34], [35] as

$$\pi\left(\begin{bmatrix}\epsilon_r' \\ \epsilon_r''\end{bmatrix}\right) \propto \exp\left\{-\frac{1}{2}\begin{pmatrix}\epsilon_r' - \eta_{\epsilon_r'} \\ \epsilon_r'' - \eta_{\epsilon_r''}\end{pmatrix}^\top \begin{pmatrix}\Gamma_{\epsilon_r'} & \Gamma_{\epsilon_r'\epsilon_r''} \\ \Gamma_{\epsilon_r''\epsilon_r'} & \Gamma_{\epsilon_r''}\end{pmatrix}^{-1} \times \begin{pmatrix}\epsilon_r' - \eta_{\epsilon_r'} \\ \epsilon_r'' - \eta_{\epsilon_r''}\end{pmatrix}\right\}. \quad (22)$$

The terms $\eta_{\epsilon_r'}$ and $\eta_{\epsilon_r''}$ denote the mean values of the real and imaginary parts of the dielectric constant, respectively. The matrices $\Gamma_{\epsilon_r'} \in R^{N_n \times N_n}$ and $\Gamma_{\epsilon_r''} \in R^{N_n \times N_n}$ are the marginal covariance matrices. $\Gamma_{\epsilon_r'\epsilon_r''} \in R^{N_n \times N_n}$ and $\Gamma_{\epsilon_r''\epsilon_r'} \in R^{N_n \times N_n}$ are the cross-covariance matrices of real and imaginary parts of dielectric constant, which embeds their correlation. The covariance $\Gamma_{\epsilon_r} \in R^{2N_n \times 2N_n}$, assumed to be a positive definite matrix, is given as

$$\Gamma_{\epsilon_r} = \begin{pmatrix}\Gamma_{\epsilon_r'} & \Gamma_{\epsilon_r'\epsilon_r''} \\ \Gamma_{\epsilon_r''\epsilon_r'} & \Gamma_{\epsilon_r''}\end{pmatrix}_{2N_n \times 2N_n}. \quad (23)$$

1) Uncorrelated Real and Imaginary Parts: If real and imaginary parts of the dielectric constant are treated as statistically uncorrelated, i.e., $\Gamma_{\epsilon_r'\epsilon_r''} = \Gamma_{\epsilon_r''\epsilon_r'} = 0$, then the prior covariance matrix can be written as

$$\Gamma_{\epsilon_r} = \begin{pmatrix}\Gamma_{\epsilon_r'} & 0_{N_n} \\ 0_{N_n} & \Gamma_{\epsilon_r''}\end{pmatrix}_{2N_n \times 2N_n} \quad (24)$$

where 0_{N_n} is an $N_n \times N_n$ zero matrix. The moisture field variation inside the foam is assumed to be smooth. Here, such a random field [36] can be generated using squared-exponential (SE) covariance function [37], which can account for the inhomogeneities. In general, the SE structure in 2-D is defined as

$$C_{ij} = \exp\left(-\frac{1}{2}\left(\frac{\left\|\mathrm{x}_i - \mathrm{x}_j\right\|^2}{c_\mathrm{x}^2} + \frac{\left\|\mathrm{y}_i - \mathrm{y}_j\right\|^2}{c_\mathrm{y}^2}\right)\right) \quad (25)$$

where c_x and c_y are characteristic length components and $i, j = 1, \ldots, N_n$. In practice, the characteristic lengths affect the moisture distribution (smoothness) in the x and y directions, respectively, Thus, (24) becomes

$$\Gamma_{\epsilon_r} = \begin{pmatrix}\sigma_{\epsilon_r'}^2 C & 0_{N_n} \\ 0_{N_n} & \sigma_{\epsilon_r''}^2 C\end{pmatrix}_{2N_n \times 2N_n} \quad (26)$$

where $\sigma_{\epsilon_r'}$ and $\sigma_{\epsilon_r''}$ are the standard deviations for the real and imaginary parts of the dielectric constant, respectively. These standard deviation values are multiplied with the SE covariance function, so as to control its overall amplitude variation. The values are chosen based on what knowledge of the unknown parameters is available prior to any measurements.

2) Correlated Real and Imaginary Parts: Consider that the real and imaginary parts of the dielectric constant are assumed statistically correlated. This implies that the cross-covariance terms $\Gamma_{\epsilon_r'\epsilon_r''} \neq 0$ and $\Gamma_{\epsilon_r''\epsilon_r'} \neq 0$ are required to form the covariance structure in (23). However, to find cross-variances matrices, dependence between the two random variables should be known. Herein, to establish the correlation between the random variables and form the prior covariance structure, we use sample-based densities.

In sample-based densities, we make use of a large set of previously/numerically obtained samples of the random variable in question. These datasets are known as samples. Assume that $\pi = \pi(\epsilon_r)$ is the probability density of a random variable ϵ_r, and we have a large database χ of size K and contain realizations of ϵ_r

$$\chi = \left\{ \begin{pmatrix} \epsilon_r' \\ \epsilon_r'' \end{pmatrix}_1, \begin{pmatrix} \epsilon_r' \\ \epsilon_r'' \end{pmatrix}_2, \begin{pmatrix} \epsilon_r' \\ \epsilon_r'' \end{pmatrix}_3, \ldots, \begin{pmatrix} \epsilon_r' \\ \epsilon_r'' \end{pmatrix}_K \right\} \tag{27}$$

where K is the total number of samples. The aim is to approximate $\pi(\epsilon_r)$ based on the χ. For this, we calculate the sample mean

$$\eta_{\epsilon_r} = \begin{pmatrix} \eta_{\epsilon_r'} \\ \eta_{\epsilon_r''} \end{pmatrix} \approx \frac{1}{K} \sum_{j=1}^{K} \begin{pmatrix} \epsilon_r' \\ \epsilon_r'' \end{pmatrix}_j \tag{28}$$

and sample covariance

$$\Gamma_{\epsilon_r} \approx \frac{1}{K} \sum_{j=1}^{K} \begin{pmatrix} \epsilon_r' \\ \epsilon_r'' \end{pmatrix}_j \begin{pmatrix} \epsilon_r' \\ \epsilon_r'' \end{pmatrix}_j^T - \begin{pmatrix} \eta_{\epsilon_r'} \\ \eta_{\epsilon_r''} \end{pmatrix} \begin{pmatrix} \eta_{\epsilon_r'} \\ \eta_{\epsilon_r''} \end{pmatrix}^T. \tag{29}$$

The dielectric constant values for the samples are generated numerically using the data from the dielectric characterization of the polymer foam in the laboratory environment. In the dielectric characterization, a small cylindrical shape volume of the foam is characterized using a cavity perturbation technique at room temperature to obtain the complex dielectric value for different levels of moisture content. The developed dielectric measurement system is shown in Fig. 2. The foam sample is located in a quartz tube to have a stable position inside the cavity. Both sides of the cavity are terminated to a small iris of 10 mm width and the same height as the WR340 waveguides [38]. The moisture content is calculated based on the wet basis, that is,

$$M = \frac{W_m - W_d}{W_m} \times 100 \tag{30}$$

where M is the moisture percentage, W_m is the weight of the foam sample after adding the water, and W_d is the weight of the dry sample. At the first step, we obtained the dielectric constant associated with the 0% moisture level. Then, a certain amount of water is added manually, and the dielectric constant is recorded in each level. The real part of relative dielectric constant was found to be in the range of 1.164 and 3.255,

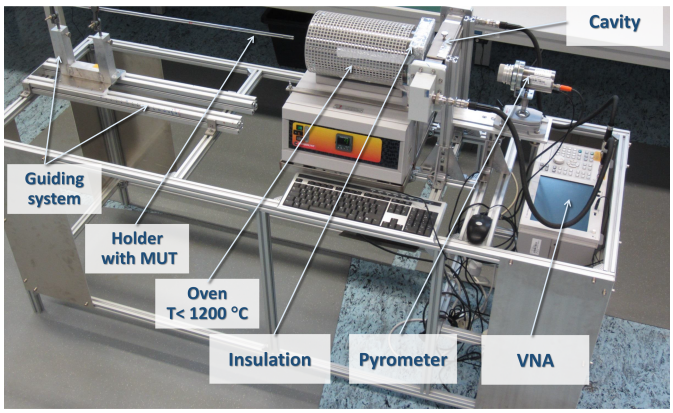

Fig. 2. Experimental setup of the cavity-perturbation [38] method for dielectric characterization of the foam.

TABLE I
MATERIAL MODEL PARAMETERS

	$\bar{a}_\theta$	δ_{a_θ}	b_θ	δ_{b_θ}
ϵ_r'	1.085	0.01591	0.01256	0.00062
ϵ_r''	0.03021	0.0025	0.02249	0.0009

and the imaginary part varying between 0.017–0.276 for *wet basis* moisture content from 0% to 80%, respectively. After the characterization, the relationship between the *wet-basis* moisture content M_{meas} and its corresponding dielectric value is obtained using curve fitting and is given as [10], [39]

$$\theta = \bar{a}_\theta \exp\left(\bar{b}_\theta M_{\text{meas}}\right) \tag{31}$$

where $\theta = \{\epsilon_r', \epsilon_r''\}$ denotes the material parameters. The values for the mean terms $\bar{a}_\theta$ and $\bar{b}_\theta$ are provided in Table I. The variables δ_{a_θ} and δ_{b_θ} are the standard deviation terms and denote the uncertainties in the curve fitting.

In order to create the dataset χ containing different moisture content realizations, the experimentally obtained mapping $M_{\text{meas}} \rightarrow \{\epsilon_r', \epsilon_r''\}$ is applied. To generate simulated moisture samples, the uncertainties in the dielectric characterization is also considered, and hence, (31) is replaced as

$$\theta = a_\theta \exp\left(b_\theta M\right) \tag{32}$$

where a_θ and b_θ are random variables such that $a_\theta \sim \mathcal{U}(\bar{a}_\theta - \delta_{a_\theta}, \bar{a}_\theta + \delta_{a_\theta})$ and $b_\theta \sim \mathcal{U}(\bar{b}_\theta - \delta_{b_\theta}, \bar{b}_\theta + \delta_{b_\theta})$, where the variable are sample from the uniform distribution $\mathcal{U}$. Numerical values for δ_{a_θ} and δ_{b_θ} are given in Table I. The moisture content distribution in each sample M can be expressed as

$$M = M^* \mathbb{1} + \delta_M L Z \tag{33}$$

where $\mathbb{1}$ is an all-ones vector, M^* and δ_M are the mean and standard deviation of the moisture content field, respectively, L is the lower triangular matrix of the Cholesky factorization of the covariance C, and Z is a standard normal random vector.

Using (32) and (33), a dataset χ with $K = 5000$ random moisture samples is created. For each sample, moisture mean and standard deviation are chosen randomly. Also, the characteristic lengths in each sample were randomized.

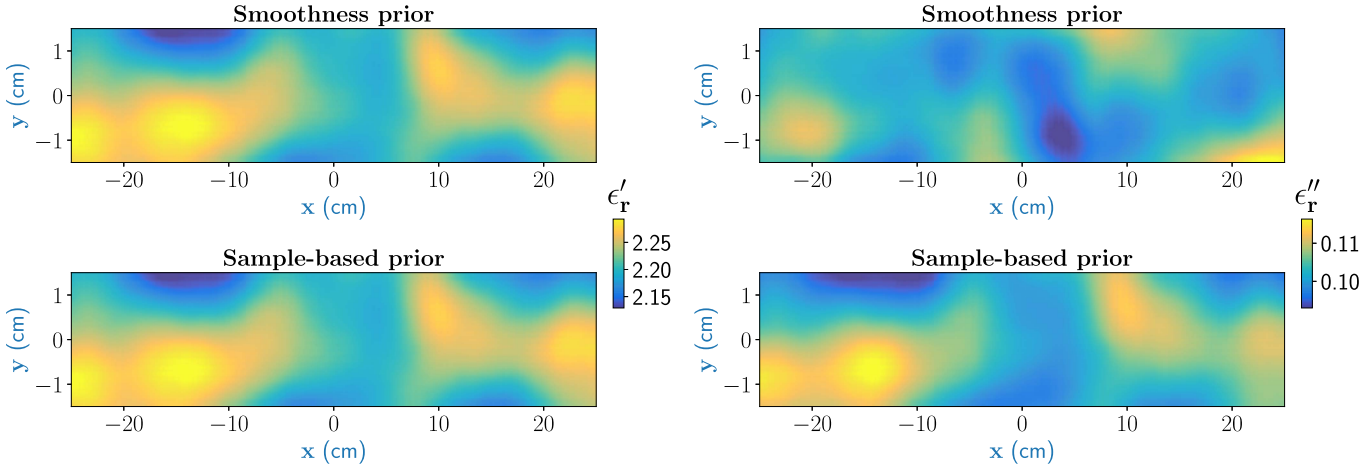

Fig. 3. Real (left) and imaginary (right) parts of the dielectric constant for samples drawn from uncorrelated smoothness and sample-based prior models.

Algorithm 1 Steps for Generating Samples for the Correlated Sample-Based Prior Model. Note That, to Ensure the Positive Definiteness for Matrix C, a Small Diagonal Component Is Added

1: $M^* \sim \mathcal{U}(0, 80)$ %, $\delta_M \sim \mathcal{U}(2, 20)$ %
2: $c_{\mathrm{x}} \sim \mathcal{U}(\mathrm{x_{min}}, \mathrm{x_{max}})$, $c_{\mathrm{y}} \sim \mathcal{U}(\mathrm{y_{min}}, \mathrm{y_{max}})$
3: Evaluate $C = \mathrm{Covariance}(c_{\mathrm{x}}, c_{\mathrm{y}}, \mathrm{x}, \mathrm{y})$ using (25)
4: $L = \mathrm{Cholesky}(C)$
5: $M = M^* \,\mathrm{ones}(N_n) + \delta_M L \,\mathrm{randn}(N_n)$
6: Calculate ϵ'_r, ϵ''_r using (32)

A pseudocode for generating a sample is given in the following, where the terms $\mathrm{x_{min}} = 0$ cm, $\mathrm{x_{max}} = 50$ cm, $\mathrm{y_{min}} = 0$ cm, and $\mathrm{y_{max}} = 3$ cm denote the minimum and maximum dimensions in the x and y directions of the foam domain, respectively.

Using the dataset, in which each sample is stacked in a vector form [see (8)], we calculated (28) and (29) using MATLAB built-in mean and covariance functions. The new prior covariance structure, from here on, is known as the sample-based prior model. The samples (or realization) from this prior density can be generated as

$$\epsilon_r = \eta_{\epsilon_r} + L_{\epsilon_r} Z. \tag{34}$$

A randomized draw from the sample-based prior model is shown in Fig. 3 (right). Also, the same sample when we ignore the cross-covariance terms is shown in Fig. 3 (left). It is evident that, with the sample-based prior model, similar spatial variations are seen in the real and imaginary parts. However, with the neglected cross-covariance matrices, real and imaginary parts show different variations. In the next section, we present numerical examples that show how the choice of two priors affects the MAP estimation and overall estimation accuracy. It should be emphasized that, to evaluate the MAP estimate with uncorrelated parameters, we have used (26) instead of sample-based prior covariance with cross-covariance terms treated as zero.

V. Numerical Results

In this section, we evaluate the performance of the MAP estimates with the smoothness prior and sample-based prior for different moisture scenarios and levels. The imaging algorithm is tested with three cases where a high moisture distribution is tested in the first case. In the second case, it is assumed that moisture distribution is piecewise constant. For the third case, considering practical interest, the foam top surface geometry is assumed rough instead of the planar, and the moisture is modeled as a hot spot (has more moisture than the surrounding area). To generate the numerical measurement data from the MWT setup shown in Fig. 1, a finite element method (FEM)-based COMSOL simulation tool is chosen. The scattered electric field data are generated at a frequency of 8.3 GHz and stored in a matrix of size 12×12. Also, we added noise of 3% of the peak value of the numerical scattered field to the data. Note that the lower frequency point is chosen from X-band as it presents low degree of nonlinearity for the inverse scattering problem [40], [41] and computational efficiency.

As for the observation model $\mathscr{F}(\epsilon_r)$, we choose the method of moment (MoM) computation [42] with a pulse basis and point-matching testing function. For the MoM computation at 8.3 GHz, we assume that the imaging domain Ω_{foam} is discretized into 80×20 uniform rectangular pixels along the x and y directions, respectively. Here, the pixel size is chosen to be of size $\lambda/6$, so as to achieve sufficient numerical accuracy for the MoM solver (in comparison to the COMSOL solver). Thus, the total number of unknowns in the imaging domain, i.e., the real and imaginary part of the dielectric constant, for estimation becomes 3200. Note that a different solver is chosen for synthetic data generation to ignore "inverse crime," [12], i.e., the use of the same grid settings or numerical model for data generation and observation model. Otherwise, the same grid setting or the numerical model may potentially lead to a situation where severe modeling errors are ignored, hence giving a false impression on the accuracy of the estimates.

To calculate the MAP estimates with the smoothness prior, we set prior $\sigma_{\epsilon'_r} = 1$, and $\sigma_{\epsilon''_r} = 0.1$. The mean value η_{ϵ_r} in the prior is set to dielectric constant of the dry foam,

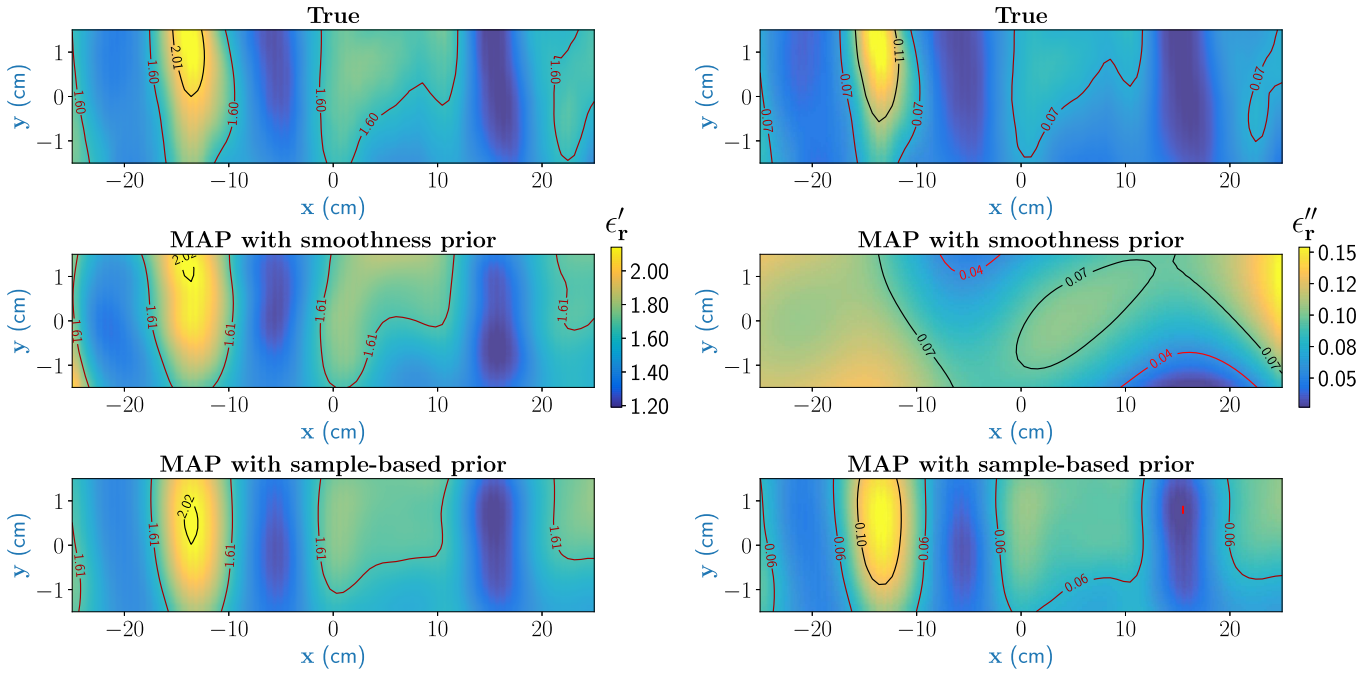

Fig. 4. High moisture case: MAP estimates with smoothness prior and sample-based prior model with real part (left) and imaginary part (right) of the dielectric constant. To highlight the dielectric constant values, contour is added.

i.e., $1.16 - j0.01$. For the sample-based prior, the prior covariance structure evaluated from the database is directly used to calculate the MAP estimates. For our simulation study, $\sigma_{\mathbb{R}}$ and $\sigma_{\mathbb{I}}$ are set to 3% of the peak value of the numerical scattered field data. To start the iteration, the value of ϵ_{r_0} is set to the dielectric constant of the dry foam, i.e., $\epsilon_{r_0} = 1.16 - 0.01i$ and $\alpha = 0.25$ are sets of all the reconstructions. The iterations are terminated, following the stopping criteria $Q(\epsilon_{r_{\ell+1}}) < Q(\epsilon_{r_\ell})$, where $Q(\epsilon_{r_\ell})$ is the norm term defined in (18). The reconstruction algorithm is implemented in MATLAB 2018b and takes approximately or less than 1 min per image. All computations were performed on a local computer with the configuration of 32 GB access memory, Intel Core(TM) i7-7820HQ central processing unit, and Nvidia Quadro M2200 graphics processing unit.

A. Smooth Moisture Variation

In the first set of experiments, numerical scattered electric field measurement data for a high moisture scenario are generated using (32) and (33). The MAP estimation with smoothness prior model and sample-based prior model is shown in Fig. 4. It can be seen that, with both the priors, the real part is estimated fairly well. However, the estimation of the imaginary part is much more accurate with the sample-based prior model with certain moisture regions being clearly indicated.

Post reconstruction, we also plotted the MAP estimate for a fixed value y = 0 cm along the cross section of the foam with ± 3 posterior standard deviation and compared it against the respective true cases for both the real and imaginary parts, as shown in Fig. 5. Especially, for the imaginary part, the uncertainty bound is higher when using just smoothness prior. However, this uncertainty bound is reduced for the case with sample-based prior. To quantitatively evaluate the accuracy of the reconstruction, we compared the true and estimated profile by using root mean square error (RMSE) and resemblance coefficient (RC) performance metrics. The RC parameter is calculated as

TABLE II
HIGH MOISTURE CASE

Prior	Smoothness		Sample-based	
Dielectric	ϵ'_r	ϵ''_r	ϵ'_r	ϵ''_r
RMSE (%)	1.84	31.91	1.79	8.21
RC	0.9752	0.3490	0.9771	0.9610

$$\mathrm{RC}_{\epsilon_r} = \frac{\int\int_{\Omega_{\text{foam}}} \overline{\epsilon_r^{\text{MAP}}}\,\overline{\epsilon_r^{\text{True}}}\, dx dy}{\sqrt{\int\int_{\Omega_{\text{foam}}} \left(\overline{\epsilon_r^{\text{MAP}}}\right)^2 dx dy}\sqrt{\int\int_{\Omega_{\text{foam}}} \left(\overline{\epsilon_r^{\text{True}}}\right)^2 dx dy}} \tag{35}$$

where $\overline{\epsilon_r^{\text{MAP}}} = \epsilon_r^{\text{MAP}} - \langle \epsilon_r^{\text{MAP}} \rangle$, $\overline{\epsilon_r^{\text{True}}} = \epsilon_r^{\text{True}} - \langle \epsilon_r^{\text{True}} \rangle$, and $\langle \cdot \rangle$ is the mean operator. For the RC, its values vary between 0 and 1. As the RC gets closer to 1, the MAP estimation is closer to the true profile. The RMSE and RC are calculated separately for the real and imaginary parts of the dielectric constant. Note that, to calculate these metrics, the number of pixels in the true profile is interpolated corresponding to the pixels in the estimated profile. The performance metric values for high moisture cases are shown in Table II. They are compared separately for the real and imaginary parts for the two prior models. It is clear from RC and RMSE values that the overall accuracy of the MAP estimate has improved with the sample-based prior model in both cases.

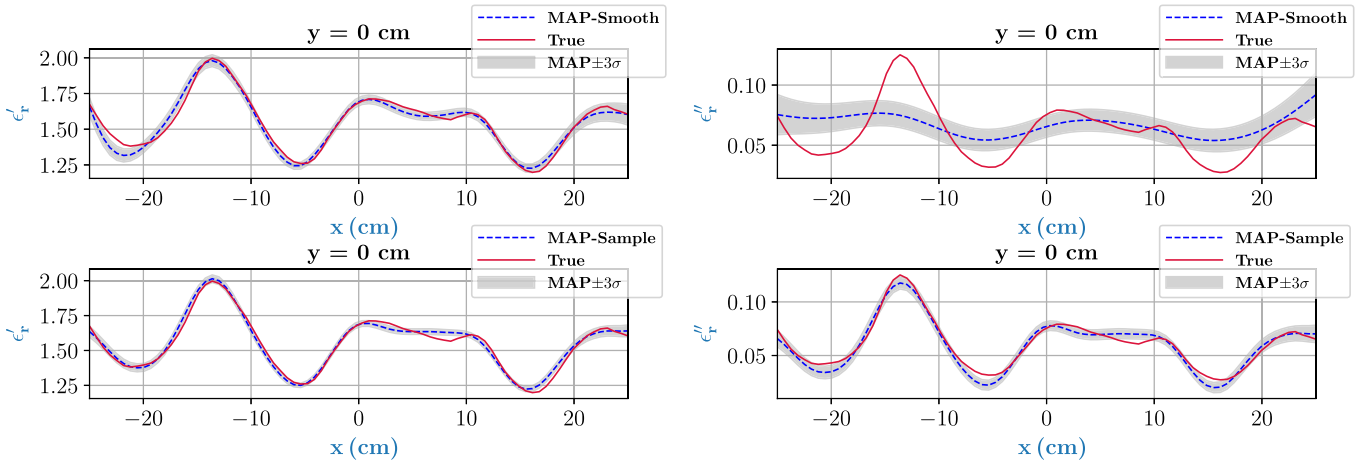

Fig. 5. Comparison between the true profile and MAP estimate for a high moisture case along the cross section of the foam y = 0 cm. The real part (left) and imaginary part (right) of the estimates are compared for smooth (top) and sample based prior (bottom), respectively. The light gray color denotes ±3 posterior standard deviation, denoted as σ.

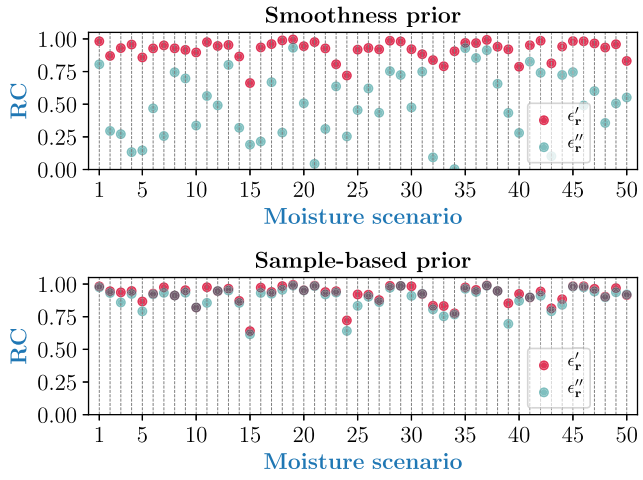

Fig. 6. Representation of RC evaluated for reconstructed distribution with smoothness prior (top) and sample-based prior (bottom) for 50 moisture scenarios. The vertical dashed lines indicate the serial number for the moisture scenario.

Furthermore, we also tested the two prior models on 50 different smoothly distributed moisture scenarios and evaluated the corresponding RC parameter, as shown in Fig. 6. Note that the RC metric is chosen for better representation purposes only. For most of the selected scenarios, significant improvement can be seen in RC with the sample-based prior model.

B. Piecewise Homogeneous Moisture Distribution

In this case, the moisture distribution is assumed piecewise homogeneous in the foam. The moisture area is given the value $\epsilon_{r_{\text{moisture}}} = 1.557 - j0.05$, and the rest of the foam is assumed dry with $\epsilon_{r_{\text{dry}}} = 1.16 - j0.01$. It should be emphasized that the primary goal is not to estimate the exact shape of the moisture area. This special case is taken considering practical interest where the moisture is sometimes located in bulk in one portion of the foam. Also, this case will test the generalization capabilities of the algorithm. As it breaks the smoothness assumption, which is otherwise present in the dataset of

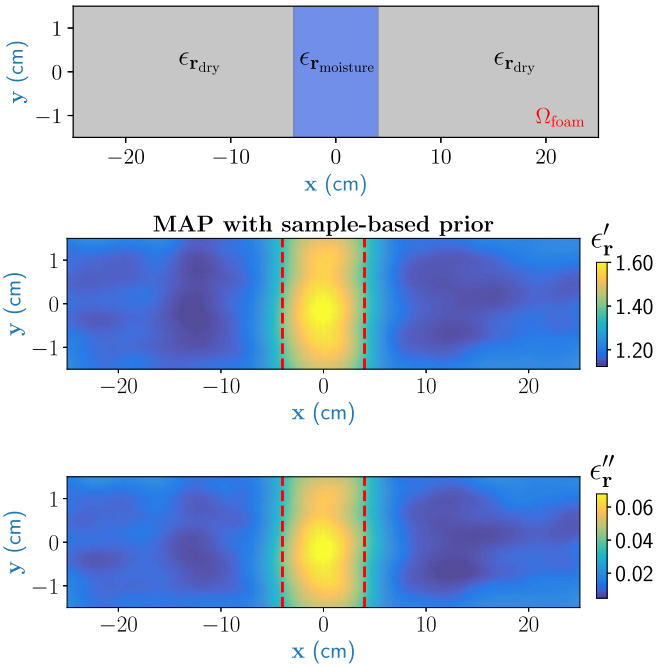

Fig. 7. MAP estimates for the piecewise homogeneous moisture scenario (top) with sample-based prior with real (middle) and imaginary parts (bottom) of the dielectric constant. The red dashed lines indicate the true boundary of the moisture profile.

samples used to build the sample-based prior covariance structure, the MAP estimates from the sample-based prior model are shown in Fig. 7 along with the true moisture distribution. We observe that both the estimated real and imaginary parts of the dielectric constant indicate the same presence of moisture and are well-estimated. This is also evident from the performance metrics shown in Table III. In the MAP estimates with smoothness-based prior, the imaginary part showed the wrong location of the moisture and hence not shown.

C. Random Rough Surface

So far, the foam with a planar surface is considered for moisture detection during an industrial process. However, it

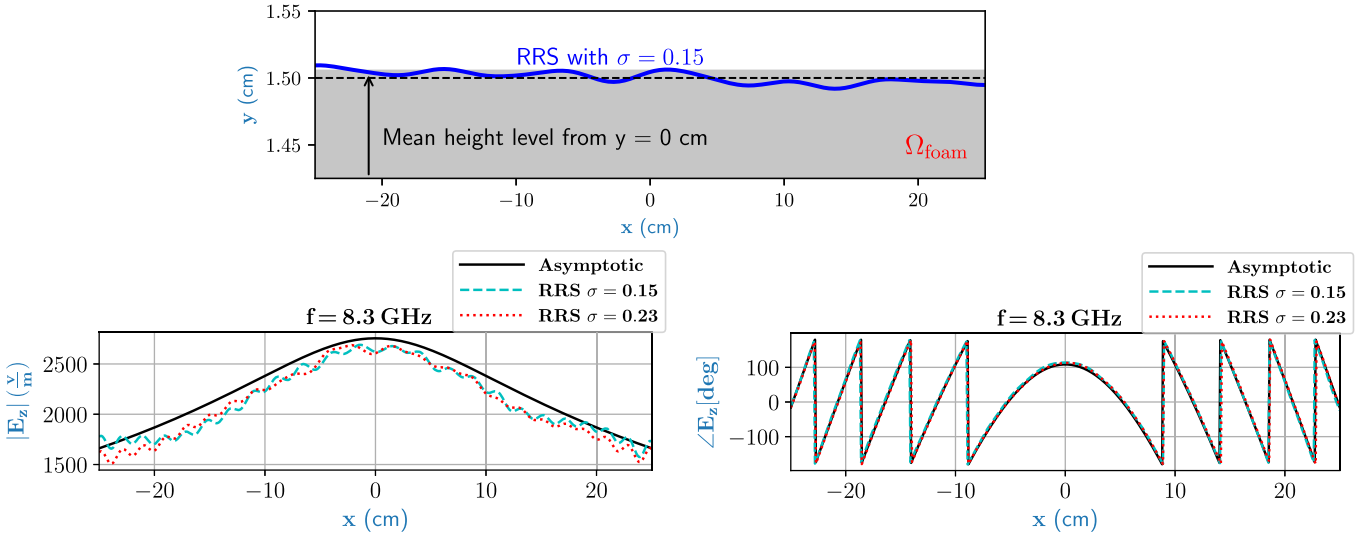

Fig. 8. Top figure shows the top surface of the foam with considered roughness and its mean height. Asymptotic electric fields magnitude (bottom left) and phase (bottom right) compared with the FEM results of a rough surface with an σ of 0.15 and 0.23 are probed at y $= -0.5$ cm and -25 cm $\leq$ x $\leq$ 25 cm with shown for the line source number 4 located at y $= 11.5$ cm.

TABLE III
PIECEWISE HOMOGENEOUS CASE

Prior	Smoothness		Sample-based	
Dielectric	ϵ_r'	ϵ_r''	ϵ_r'	ϵ_r''
RMSE (%)	5.2	67.82	4.0582	22.83
RC	0.9017	0.5637	0.9398	0.9362

has been observed that dielectric foam as a porous material can also have some uncertainty on the surface. In order to investigate the effect of the roughness of the surface, we consider a dielectric foam with a randomly rough surface (RRS) at the top. The random roughness is modeled [43] as follows:

$$\mathrm{y(x)} = \sum_{m=-M}^{M} m^{-\beta} G_m \cos(2\pi m \mathrm{x} + U_m) \tag{36}$$

where m is the integer number representing the spatial frequency, β denotes the spectral exponent, $G_m \sim \mathcal{N}(0, \sigma)$ is sampled from a Gaussian distribution, and $U_m \sim \mathcal{U}(0, 2\pi)$ is sampled from the uniform distribution. The random rough surface is characterized here by the following parameters: $\sigma = 0.15$ and $\beta = 0.8$. To obtain the scattered field, a hot-spot with 40% moisture $(1.3785 - j0.0432)$ with radius 1 cm at position (15 cm, 0 cm) is considered inside the foam with permittivity $1.16 - j0.01$ and a moderate rough surface with mentioned parameters.

In Fig. 8, for one sample frequency, i.e., f $= 8.3$ GHz, the real and imaginary parts of the electric field of FEM and asymptotic fields are compared [44] for a dry foam with two different degrees of roughness. It should be noted, in order to obtain the asymptotic expression for the rough media, it is assumed that the fluctuation in the top surface is zero (i.e. root mean square (rms) height). Moreover, in the forward model, the top surface is given the average distance from each antennas to the top surface of the foam, i.e., $h = \langle h_i \rangle$ and $i = 1, 2, \ldots, N/2$. The distance from the bottom antennas to the bottom surface of the foam is considered unique (has only one value). We observed that, in the MAP estimate, as shown in Fig. 9, with the smoothness prior, the imaginary part is indicating the presence of a strong artifact. However, in the estimated imaginary part with sample-based prior, strong presences of only one-hot spot is favorable. However, with both prior models, the shadow image due to the roughness of the surface is also visible.

VI. EXPERIMENTAL RESULTS

In this section, the sample-based prior model is tested on the scattering electric field data from our experimental MWT data for a wet-spot moisture case in a planar foam of size $50 \times 7.6 \times 75$ cm. The MWT experimental prototype shown in Fig. 10 consists of 12 WR90 open-ended waveguide antennas (with a VSWR 1.03 : 1). The distance of the top and bottom antenna to the top and bottom surface of the polymer foam is 8 cm, and the center-to-center distance between two adjacent antennas is 5 cm. The top and bottom antennas are resided in free-space from -12.5 cm to $+12.5$ cm along the x-axis. For data acquisition, antennas are connected to the Agilent N5224A vector network analyzer (VNA) via a P9164C 2×16 USB solid-state switch matrix with the maximum power level of 5 dBm. It should be noted that a waveguide calibration is performed to remove the unwanted reflections. Moreover, the MWT setup is surrounded by absorbers to increase the signal-to-noise ratio. Phase stable cables (offering phase stability of 3° at the maximum frequency) are used for the connections between the measurement devices and the antennas. Communication between the controlling computer, VNA, and the switch is provided using the Ethernet cable. The data acquisition process is entirely automated using MATLAB R2018b. For each foam sample, 12×12 data points (S-parameter measurements) were collected at 8.3 GHz using

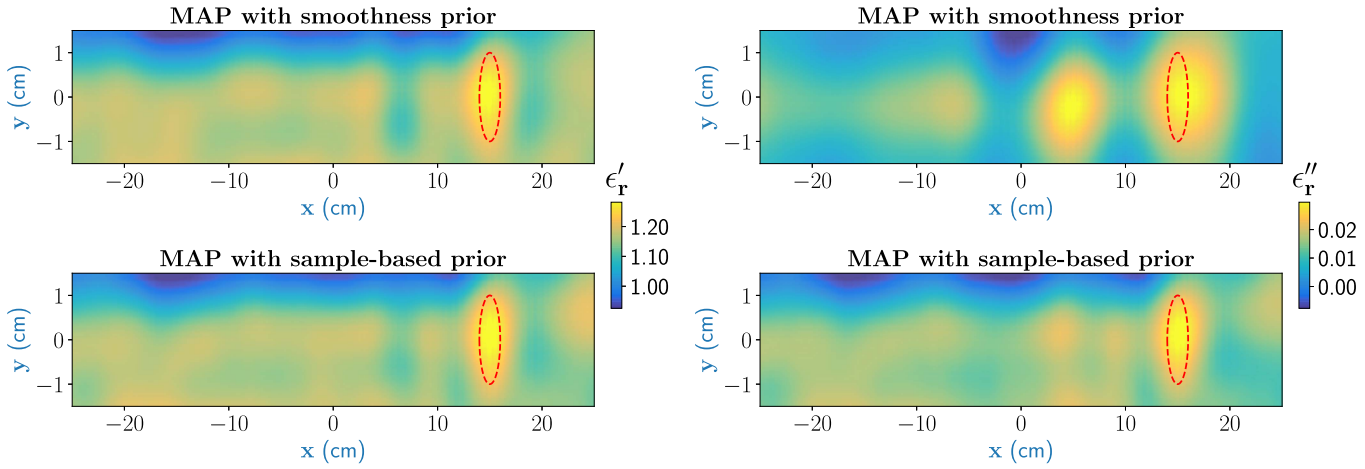

Fig. 9. Reconstructions with smoothness prior (first row) and sample-based prior (second row) of a hot-spot area embedded inside the foam with an assumed rough top surface with $\sigma = 0.15$.

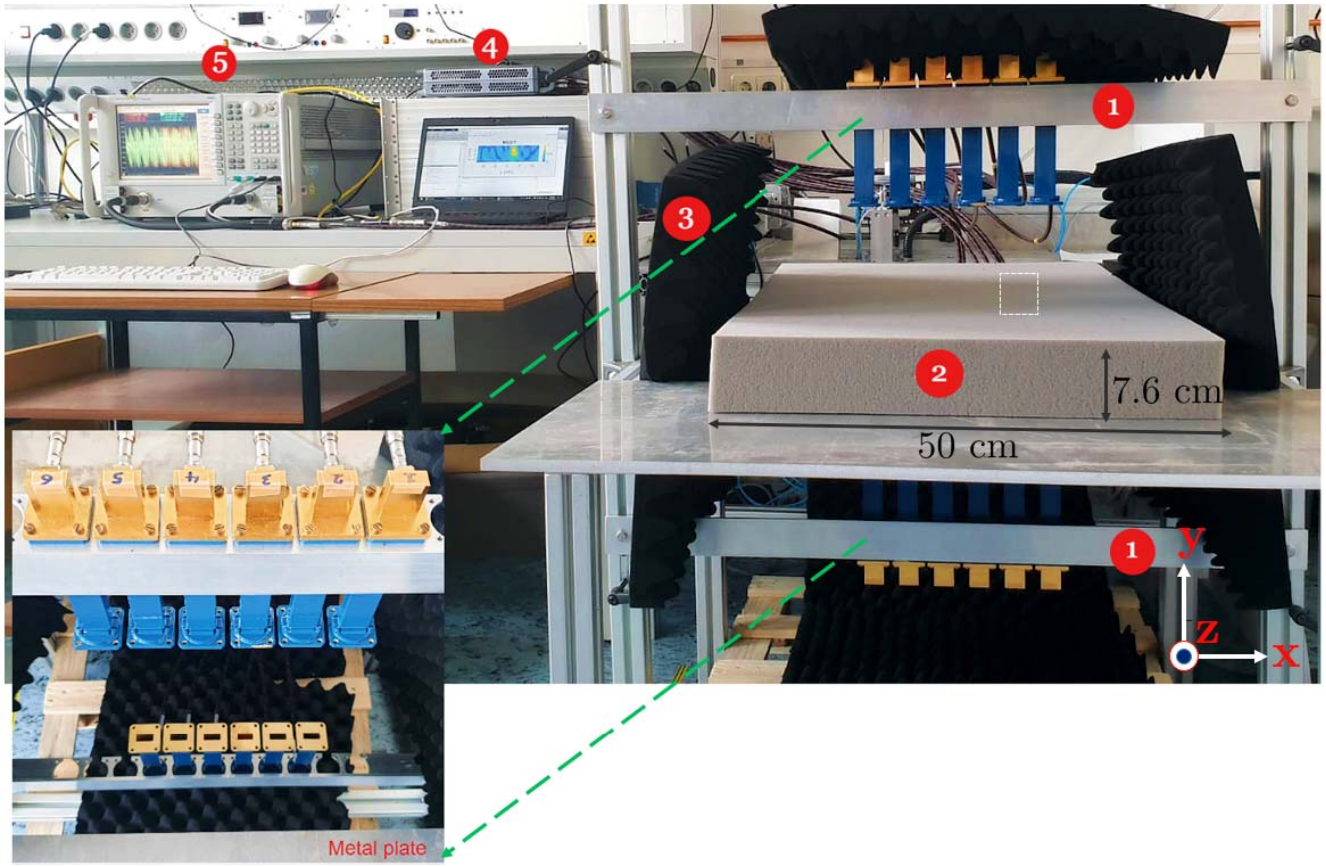

Fig. 10. Experimental setup of the MWT system prototype at the KIT Laboratory, Germany. The MWT system consists of X-band open-ended waveguide antennas as sensors and is indicated by number Tag 1. The alignments of the top and bottom antennas are shown in the bottom left by the green arrow, and the portion of the metal plate is removed to enable wave propagation between the top and bottom antennas. The polymer foam is shown by number Tag 2 and surrounded by absorbers, as shown by number Tag 3. The measurement data acquisition setup consists of the solid switch and VNA that are denoted by number Tags 4 and 5, respectively. The location plane of the test target is shown in right by white dash lines.

an IF bandwidth of 500 Hz. The approximate time for data acquisition was about 40 sec.

To create the wet-spot moisture target, a spherical foam of diameter 2.5 ± 0.1 cm and with 46% wet-basis moisture level ($\epsilon_r \approx 2.0 - 0.085i$) is chosen. An approximate location of the target inside the foam is centered at $(-9$ cm, 1.55 cm, 0 cm). We follow similar steps described in Section V to obtain the MAP estimates from the measurement data. Only the standard deviations of the measurement noise [see (21)] need to be changed and are calculated for 8.3 GHz frequency point

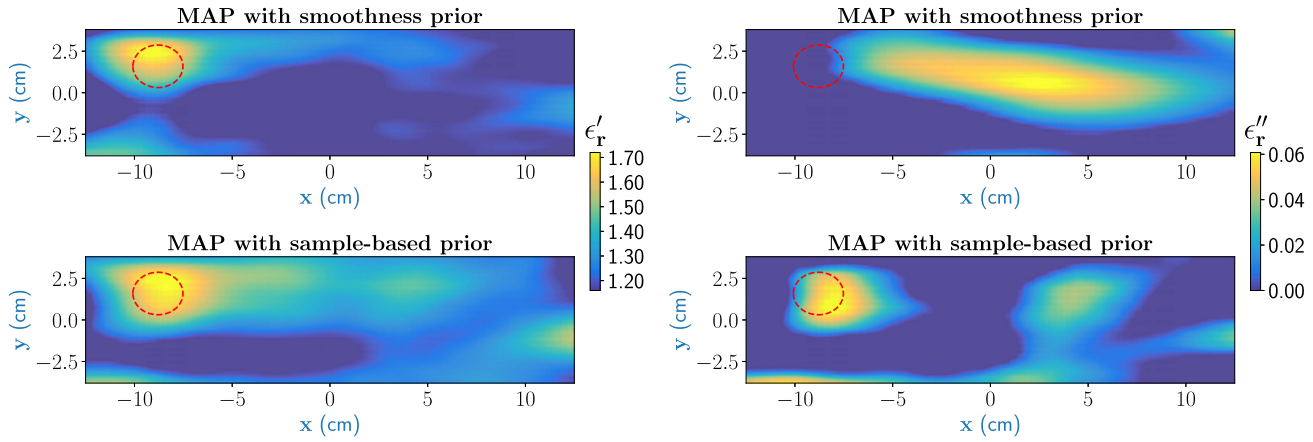

Fig. 11. Reconstructions with smoothness prior (left) and sample-based prior (right) of a wet-spot area embedded inside the foam. The red dashed line indicates the true mean location of the target.

following the approach used in [45]. In the forward model, the antennas are modeled as line sources, and the electric field data E_{MoM} are converted to equivalent scattering matrix (in terms of S-parameter) S_{MoM} through calibration with respect to dry foam response $S_{\text{scat}_{\text{dry}}}$ as

$$S_{\text{MoM}} = \frac{S_{\text{scat}_{\text{dry}}}}{E_{\text{MoM}_{\text{dry}}}} \odot E_{\text{MoM}}. \tag{37}$$

The MAP estimate with the smoothness prior and sample-based prior is shown in Fig. 11 for the selected x-y plane at z = 0 cm. With the smoothness model, the location of the target and its value are satisfactorily estimated in the real part. However, the imaginary part shows completely different spatial variations of the moisture distribution in the foam. With the sample-based prior, a significant improvement in the MAP estimation is observed. It is clear that, with this sample-based prior approach, the obtained MAP estimates offer a good reconstruction accuracy in comparison to the smoothness prior model.

VII. Conclusion and Discussion

In this work, we used microwave tomography to estimate the moisture distribution (as dielectric constant) in a polymer foam using the Bayesian inversion framework. The imaging modality will be integrated to derive intelligent control approach for an industrial microwave drying system. It is shown that, when real and imaginary parts are treated uncorrelated in the smoothness-based prior model, obtained dielectric values can be conflicting and incorrect i.e., there is some imbalance between the real and imaginary parts of the dielectric constant. Thus, we proposed a sample-based prior model to correctly reconstruct both the real and imaginary parts of the dielectric constant and the corresponding correlation between them. To construct the sample-based prior model, we use a large dataset consisting of simulated moisture samples to evaluate the prior mean and build the prior covariance structure. In each sample, moisture values are chosen based on the parametric model obtained from the dielectric characterization of the foam. The proposed approach is tested with 2-D numerical microwave tomography data obtained in the X-band frequency for the considered moisture scenarios. The results presented show that a significant improvement in the estimation result is achieved with the sample-based prior model in comparison to the smoothness prior model. Also, two performance metrics, namely, the RC and RMSE, clearly highlight the effectiveness of the sample-based prior model on the reconstruction accuracy. Furthermore, the developed algorithm is tested on the MWT experimental prototype data. The results obtained with sample-based prior indicate that the estimated moisture distribution is very close to the true moisture scenarios considered in comparison to the smoothness prior.

We observed that the real and imaginary parts in the MAP estimation are slightly underestimated, which may be caused due to the modeling errors. Together with the source modeling error, this discrepancy might be caused due to the 2-D versus 3-D Green's function mismatch when the geometry of the target is no longer independent of the z-coordinates. In essence, these errors are very significant for the case when spherical geometries are assumed for the wet spots in comparison to infinite extended scatterer cases (where the general performance of the 2-D forward model with line sources is good). A detailed discussion was provided in [46] for medical imaging applications but is equally applicable for our application as well. Nonetheless, the source model errors remain persistent in our study. Thus, one way to improve the reconstructions is by using the Bayesian inversion approach in conjunction with the approximation error scheme [4], which can accommodate statistics of these errors resulting in better estimates. Therefore, a Bayesian approximation error [47] scheme will be employed to further improve the microwave tomography estimation. In the industrial drying system, the foam temperature will be higher than the room temperature at the exit. Therefore, dielectric characterization of the foam with wet-basis moisture levels at different temperatures is our next task. In this article, the real measurements are done with the static case where the influence of the conveyor belt is not considered. Therefore, future work will be related to doing dynamic measurements where the foam will be under

movement, and the estimated moisture information will be utilized in the feedforward loop of the intelligent control block of the industrial drying system. To further reduce the data acquisition time from MWT sensor setup and build fast controllers, limited-view MWT setup with statistical inversion framework has been in the testing phase.

ACKNOWLEDGMENT

The authors would like to thank R. Nicholson from the University of Auckland for discussions related to joint reconstructions for the support; V. Nuss and D. Neumaier for providing an overview of the microwave drying system at the HEPHAISTOS Laboratory, Karlsruhe Institute of Technology, Germany.

REFERENCES

[1] J. A. T. Vasquez *et al.*, "Noninvasive inline food inspection via microwave imaging technology: An application example in the food industry," *IEEE Antennas Propag. Mag.*, vol. 62, no. 5, pp. 18–32, Oct. 2020.

[2] Z. Wu and H. Wang, "Microwave tomography for industrial process imaging: Example applications and experimental results," *IEEE Antennas Propag. Mag.*, vol. 59, no. 5, pp. 61–71, Oct. 2017.

[3] F. Becker *et al.*, "From visual spectrum to millimeter wave: A broad spectrum of solutions for food inspection," *IEEE Antennas Propag. Mag.*, vol. 62, no. 5, pp. 55–63, Oct. 2020.

[4] A. C. Metaxas and R. J. Meredith, "Industrial microwave heating," in *Power and Energy*. London, U.K.: Institution of Engineering and Technology, 1988. [Online]. Available: https://digital-library.theiet.org/content/books/po/pbpo004e

[5] Y. Sun, "Adaptive and intelligent temperature control of microwave heating systems with multiple sources," Ph.D. dissertation, KIT Dept. Elect. Eng. Inf. Technol., KIT Sci. Publishing, Karlsruhe, Germany, 2016.

[6] Y. V. Bykov, K. I. Rybakov, and V. E. Semenov, "High-temperature microwave processing of materials," *J. Phys. D, Appl. Phys.*, vol. 34, no. 13, pp. R55–R75, Jul. 2001, doi: 10.1088/0022-3727/34/13/201.

[7] G. Link and V. Ramopoulos, "Simple analytical approach for industrial microwave applicator design," *Chem. Eng. Process. Process Intensification*, vol. 125, pp. 334–342, Mar. 2018.

[8] M. Hosseini, A. Kaasinen, G. Link, T. Lähivaara, and M. Vauhkonen, "LQR control of moisture distribution in microwave drying process based on a finite element model of parabolic PDEs," *IFAC-PapersOnLine*, vol. 53, no. 2, pp. 11470–11476, 2020. [Online]. Available: https://www.sciencedirect.com/science/article/pii/S2405896320308879

[9] A. Omrani, R. Yadav, G. Link, T. Lähivaara, M. Vauhkonen, and J. Jelonnek, "An electromagnetic time-reversal imaging algorithm for moisture detection in polymer foam in an industrial microwave drying system," *Sensors*, vol. 21, no. 21, p. 7409, Nov. 2021. [Online]. Available: https://www.mdpi.com/1424-8220/21/21/7409

[10] R. Yadav, A. Omrani, G. Link, M. Vauhkonen, and T. Lähivaara, "Microwave tomography using neural networks for its application in an industrial microwave drying system," *Sensors*, vol. 21, no. 20, p. 6919, Oct. 2021. [Online]. Available: https://www.mdpi.com/1424-8220/21/20/6919

[11] A. Omrani, G. Link, and J. Jelonnek, "A multistatic uniform diffraction tomographic algorithm for real-time moisture detection," in *Proc. IEEE Asia–Pacific Microw. Conf. (APMC)*, Dec. 2020, pp. 437–439.

[12] J. Kaipio and E. Somersalo, *Statistical and Computational Inverse Problems*. Cham, Switzerland: Springer, 2005.

[13] M. K. Nguyen and A. Mohammad-Djafari, "Bayesian approach with the maximum entropy principle in image reconstruction from microwave scattered field data," *IEEE Trans. Med. Imag.*, vol. 13, no. 2, pp. 254–262, Jun. 1994.

[14] Y. Chen, J. Li, J. Zhuo, F. Han, and Q. H. Liu, "Fast multiparametric electromagnetic full-wave inversion via solving contracting scattering data equations optimized by the 3-D MRF model," *IEEE Trans. Microw. Theory Techn.*, vol. 68, no. 11, pp. 4515–4527, Nov. 2020.

[15] S. Caorsi, G. L. Gragnani, S. Medicina, M. Pastorino, and G. Zunino, "Microwave imaging based on a Markov random field model," *IEEE Trans. Antennas Propag.*, vol. 42, no. 3, pp. 293–303, Mar. 1994.

[16] R. Guo *et al.*, "Pixel- and model-based microwave inversion with supervised descent method for dielectric targets," *IEEE Trans. Antennas Propag.*, vol. 68, no. 12, pp. 8114–8126, Dec. 2020.

[17] R. Yadav, A. Omrani, M. Vauhkonen, G. Link, and T. Lahivaara, "Microwave tomography for moisture level estimation using Bayesian framework," in *Proc. 15th Eur. Conf. Antennas Propag. (EuCAP)*, Mar. 2021, pp. 1–5.

[18] A. Omrani, R. Yadav, G. Link, M. Vauhkonen, T. Lahivaara, and J. Jelonnek, "A combined microwave imaging algorithm for localization and moisture level estimation in multilayered media," in *Proc. 15th Eur. Conf. Antennas Propag. (EuCAP)*, Mar. 2021, pp. 1–5.

[19] G. Ferraiuolo and V. Pascazio, "The effect of modified Markov random fields on the local minima occurrence in microwave imaging," *IEEE Trans. Geosci. Remote Sens.*, vol. 41, no. 5, pp. 1043–1055, May 2003.

[20] R. Autieri, G. Ferraiuolo, and V. Pascazio, "Bayesian regularization in nonlinear imaging: Reconstructions from experimental data in nonlinearized microwave tomography," *IEEE Trans. Geosci. Remote Sens.*, vol. 49, no. 2, pp. 801–813, Feb. 2011.

[21] A. P. Dempster, N. M. Laird, and D. B. Rubin, "Maximum likelihood from incomplete data via the EM algorithm," *J. Roy. Statist. Soc., B Methodol.*, vol. 39, no. 1, pp. 1–38, 1977. [Online]. Available: http://www.jstor.org/stable/2984875

[22] M. A. Islam, A. Kiourti, and J. L. Volakis, "A novel method to mitigate real–imaginary image imbalance in microwave tomography," *IEEE Trans. Biomed. Eng.*, vol. 67, no. 5, pp. 1328–1337, May 2020.

[23] M. Ostadrahimi, P. Mojabi, A. Zakaria, J. LoVetri, and L. Shafai, "Enhancement of Gauss–Newton inversion method for biological tissue imaging," *IEEE Trans. Microw. Theory Techn.*, vol. 61, no. 9, pp. 3424–3434, Sep. 2013.

[24] P. Mojabi and J. LoVetri, "A prescaled multiplicative regularized Gauss-Newton inversion," *IEEE Trans. Antennas Propag.*, vol. 59, no. 8, pp. 2954–2963, Aug. 2011.

[25] R. Yadav, A. Omrani, M. Vauhkonen, G. Link, and T. Lähivaara, "Complex-permittivity estimation of a polymer foam using microwave tomography for the application of microwave drying," in *Proc. AMPERE 8th Int. Conf. Microw. High Freq. Appl.*, Sep. 2021, pp. 42–47.

[26] J. Richmond, "Scattering by a dielectric cylinder of arbitrary cross section shape," *IEEE Trans. Antennas Propag.*, vol. AP-13, no. 3, pp. 334–341, May 1965.

[27] S. Caorsi, G. L. Gragnani, and M. Pastorino, "Two-dimensional microwave imaging by a numerical inverse scattering solution," *IEEE Trans. Microw. Theory Techn.*, vol. 38, no. 8, pp. 980–981, Aug. 1990.

[28] N. Joachimowicz, C. Pichot, and J. P. Hugonin, "Inverse scattering: An iterative numerical method for electromagnetic imaging," *IEEE Trans. Antennas Propag.*, vol. 39, no. 12, pp. 1742–1753, Dec. 1991.

[29] X. Chen, *Computational Methods for Electromagnetic Inverse Scattering*. Singapore: Wiley, 2018.

[30] M. Ostadrahimi *et al.*, "Analysis of incident field modeling and incident/scattered field calibration techniques in microwave tomography," *IEEE Antennas Wireless Propag. Lett.*, vol. 10, pp. 900–903, 2011.

[31] M. Haynes and M. Moghaddam, "Multipole and S-parameter antenna and propagation model," *IEEE Trans. Antennas Propag.*, vol. 59, no. 1, pp. 225–235, Nov. 2011.

[32] D. Colton and R. Kress, *Inverse Acoustic and Electromagnetic Scattering Theory*. Berlin, Germany: Springer=, 1998.

[33] A. Franchois and C. Pichot, "Microwave imaging-complex permittivity reconstruction with a Levenberg–Marquardt method," *IEEE Trans. Antennas Propag.*, vol. 45, no. 2, pp. 203–215, Feb. 1997.

[34] S. M. Kay, *Fundamentals of Statistical Signal Processing: Estimation Theory*. Upper Saddle River, NJ, USA: Prentice-Hall, 1993.

[35] B. Picinbono, "Second-order complex random vectors and normal distributions," *IEEE Trans. Signal Process.*, vol. 44, no. 10, pp. 2637–2640, Oct. 1996.

[36] H. Rue and L. Held, *Gaussian Markov Random Fields: Theory and Applications (Monographs on Statistics and Applied Probability)*. London, U.K.: Chapman & Hall, 2005.

[37] C. Rasmussen and C. Williams, *Gaussian Processes for Machine Learning*. Cambridge, MA, USA: MIT Press, 2006.

[38] S. Soldatov, T. Kayser, G. Link, T. Seitz, S. Layer, and J. Jelonnek, "Microwave cavity perturbation technique for high-temperature dielectric measurements," in *IEEE MTT-S Int. Microw. Symp. Dig.*, Jun. 2013, pp. 1–4.

[39] T. Lahivaara, R. Yadav, G. Link, and M. Vauhkonen, "Estimation of moisture content distribution in porous foam using microwave tomography with neural networks," *IEEE Trans. Comput. Imag.*, vol. 6, pp. 1351–1361, 2020.
[40] O. M. Bucci, N. Cardace, L. Crocco, and T. Isernia, "Degree of nonlinearity and a new solution procedure in scalar two-dimensional inverse scattering problems," *J. Opt. Soc. Amer. A, Opt. Image Sci.*, vol. 18, no. 8, pp. 1832–1843, 2001.
[41] M. T. Bevacqua and T. Isernia, "An effective rewriting of the inverse scattering equations via Green's function decomposition," *IEEE Trans. Antennas Propag.*, vol. 69, no. 8, pp. 4883–4893, Aug. 2021.
[42] R. F. Harrington, *Field Computation by Moment Methods*. Hoboken, NJ, USA: Wiley, 1993.
[43] H.-O. Peitgen and D. Saupe, Eds., *The Science of Fractal Images*. Berlin, Germany: Springer, 1988.
[44] S. M. Moghadasi, M. Dehmollaian, and J. Rashed-Mohassel, "Time reversal imaging of deeply buried targets under moderately rough surfaces using approximate transmitted fields," *IEEE Trans. Geosci. Remote Sens.*, vol. 53, no. 7, pp. 3897–3905, Jul. 2015.
[45] C. Eyraud, A. Litman, A. Hérique, and W. Kofman, "Microwave imaging from experimental data within a Bayesian framework with realistic random noise," *Inverse Problems*, vol. 25, no. 2, Feb. 2009, Art. no. 024005, doi: 10.1088/0266-5611/25/2/024005.
[46] P. M. Meaney, K. D. Paulsen, S. D. Geimer, S. A. Haider, and M. W. Fanning, "Quantification of 3-D field effects during 2-D microwave imaging," *IEEE Trans. Biomed. Eng.*, vol. 49, no. 7, pp. 708–720, Jul. 2002.
[47] J. P. Kaipio, T. Huttunen, T. Luostari, T. Lähivaara, and P. B. Monk, "A Bayesian approach to improving the born approximation for inverse scattering with high-contrast materials," *Inverse Problems*, vol. 35, no. 8, Aug. 2019, Art. no. 084001, doi: 10.1088/1361-6420/ab15f3.

Rahul Yadav received the M.E. degree in electronics and communication engineering with a specialization in microwave engineering from the Birla Institute of Technology, Ranchi, India, in 2014. He is currently pursuing the Ph.D. degree with the Department of Applied Physics, University of Eastern Finland, Kuopio, Finland. His Ph.D. research involves the development of fast reconstruction algorithms for microwave tomography for industrial applications.

His research interests include computational electromagnetics and inverse problems.

Adel Omrani was born in Iran in 1991. He received the B.Sc. degree in electrical engineering from the University of Babol, Babol, Iran, in 2014, and the M.Sc. degree in electrical engineering from the University of Tehran, Tehran, Iran, in 2017. He is currently pursuing the Ph.D. degree in electrical engineering and information technology with the Karlsruhe Institute of Technology (KIT), Karlsruhe, Germany.

His current research interests include microwave imaging, antennas, numerical methods in electromagnetics, applied electromagnetic, and microwave engineering.

Guido Link received the Dipl.-Phys. and Dr.rer.nat. degrees in physics from the Technical University Karlsruhe, Karlsruhe, Germany, in 1990 and 1993, respectively. His diploma thesis and graduate research were devoted to the frequency and temperature-dependent dielectric characterization of low-loss ceramics and ionic crystals.

Since 1993, he has been working with the Karlsruhe Institute of Technology, Karlsruhe, in the field of high power microwave and millimeter-wave processing of materials as a Team Leader with the Institute for Pulsed Power and Microwave Technology. He authored or coauthored more than 200 contributed articles to international scientific conferences and more than 30 articles in scientific journals. He holds eight patents. His research interest includes dielectric measurements, design and simulation of microwave systems and processes, microwave-assisted sintering, curing of polymer composites, additive manufacturing, and plasma chemistry.

Marko Vauhkonen received the Ph.D. degree in physics from the University of Kuopio, Kuopio, Finland, in 1997.

He worked as a Researcher and Research Director with the University of Kuopio, until moving to Germany in 2006. He worked as a Marie-Curie Research Fellow for two years with Philips Research GmbH, Aachen, Germany. From 2008 to 2009, he worked as a CTO with a Spin-off Company Numcore Ltd. until starting as a Professor with the University of Kuopio (currently University of Eastern Finland), Department of Applied Physics, in 2009. He has published more than 100 scientific journal articles. His research interests include inverse problems, time-varying reconstruction, process tomography, and medical imaging, such as PET, SPECT, and MRI.

Timo Lähivaara received the M.Sc. degree from the University of Kuopio, Kuopio, Finland, in 2006, and the Ph.D. degree from the University of Eastern Finland, Kuopio, in 2010.

He is currently a Senior Researcher with the Department of Applied Physics, University of Eastern Finland. His research interests include computational wave problems and remote sensing.